Proceedings of the 10th International Conference on Civil Structural and Transportation Engineering (ICCSTE 2025)
July 2025 | Imperial College London Conference Center, London, United Kingdom
Paper No. 163
DOI: 10.11159/iccste25.163

Parametric Seismic Response of Base-Isolated Reinforced Concrete Silos

Piero H. Portal[1] and Victor I. Fernandez-Davila[1]
[1] School of Civil Engineering, Peruvian University of Applied Sciences
Av. Alonso de Molina, 1611, Lima, Peru
u20201b377@upc.edu.pe; pccivfer@upc.edu.pe

Abstract **–** Silos are vulnerable structures during severe seismic events due to their slenderness and their interaction with stored material. This investigation presents the results of a special structure that incorporates a basal seismic isolation system, such as the Triple Friction Pendulum System (TFPS). A parametric study was conducted on eight models of reinforced concrete silos to evaluate the effectiveness of TFPS isolators in mitigating the effects of various parameters on their seismic response. This research makes significant contributions by identifying parameters that affect isolated silos, providing valuable insights into their seismic behaviour. The silos were modeled and validated by comparing the forces obtained from a modal spectral analysis with analytical forces from a previous study, achieving acceptable errors for the research objectives. Finally, a nonlinear dynamic time history analysis was performed using seven seismic records, selecting one as critical due to its peak acceleration at the start. The study determined that TFPS isolators efficiently reduced the influence of the analyzed parameters in slender silos, allowing their omission in non-critical seismic events for isolated structures. Compact silos exhibited reduced effectiveness due to uplift related to their compact design and the interaction between the stored material and the structure. This necessitates a thorough evaluation of the analysed parameters. In critical case, the full slender silo exhibited no increase in seismic response due to the stiffness contribution of the stored material. Conversely, empty slender silos showed increases because the force transfer in the final Phase of TFPS isolators became critical without the stiffness contribution of the stored material. Compact silos exhibited a similar seismic response for non-critical earthquakes, but the response was amplified due to significant lateral displacements.

Keywords**:** silos, slenderness ratio, stored material-structure interaction, isolators, reinforced concrete

1. Introduction

Silos are essential structures for various industries, but their vulnerability to seismic actions has been evident in past earthquakes. This vulnerability primarily arises from uncertainties in the seismic response of the structure. Several factors contribute to this, including the interaction between the stored material and the structure, known as Stored Material-Structure Interaction (SMSI), which refers to the additional pressures exerted on the walls by the stored material. Another important factor is the Slenderness Ratio, defined as the ratio of the silo height to its diameter. These parameters lack a standardized method for quantifying the additional seismic actions they generate. Several studies have analyzed the impact of these parameters on silos, concluding that an increase in the volume of stored material leads to higher base shear forces, lateral displacements [1], dynamic pressures on the walls, and acceleration amplification factors [2], while a higher slenderness ratio results in increased shear forces, displacements, and moments [3]. However, these studies typically analyze each variable in isolation, overlooking the effects of their interaction. For instance, when comparing analyses that include soil-foundation-stored material-structure interaction [4] with those that only consider soil-stored material-structure interaction [5], discrepancies in seismic actions of 9% to 37% can be observed for the same model and seismic record. This significant variation contributes to the uncertainty in the dynamic response of silos, complicating reliable seismic design. As a solution, seismic isolators have proven effective in reducing dynamic pressures [6] and seismic forces [6-7], enabling the omission of the effects of certain parameters on the seismic response of silos. However, these studies considered only a single analysis model, which is insufficient to generalize this solution, as the effects of slenderness ratio and SMSI may be more influential in other silo configurations. Therefore, a parametric study is necessary to assess the combined impact of these two parameters on isolated silos.

Moreover, a critical question arises regarding which type of isolator is most suitable for heavy and tall structures such as silos. In this context, the Triple Friction Pendulum System (TFPS) has been identified as the most appropriate device due to its favorable dynamic performance in tall structures [8-9], its ability to mitigate uplift by defining periods between 3 and 5 seconds [10], and the direct relationship between the weight of the silo, the stiffness of the isolator, and its restoring capacity [11-12]. The advantages emphasize the importance of assessing this type of isolator in silos. On the other hand, using elastomeric isolators comes with certain challenges. These include the need for hybrid systems, the requirement for slender dimensions due to the heavy weight of the silo, which makes them susceptible to buckling, and a lower restoring capacity when compared to friction-based seismic isolators. The objective of this research is to determine the efficiency of TFPS isolators in reducing the influence of SMSI and slenderness ratio on the seismic response of base-isolated silos. This study contributes to a deeper understanding of the seismic response of isolated silos by identifying the dynamic effects of these parameters, providing valuable insights into their behavior under seismic actions.

2. Methodology

2.1. Model Characteristics

Eight reinforced concrete silo models were designed, each with a storage capacity of 11,295 tons of cement. Cement was chosen as the stored material because it is commonly found in silos in Peru, the country from which the seismic records used in this study were sourced. The slenderness ratio classification from the EN 1991-4 code [14] was applied to categorize the silos as slender ($H/D > 2$) or squat ($0.4 < H/D < 1$). Additionally, the partially filled condition was not evaluated, as it produces identical results to the filled condition [2]. Reinforced concrete rings were also added to form part of the isolation interface along with the isolators. Table 1 presents the characteristics of the analyzed models.

Table 1: Characteristics of Silo Models.

Model ID	1	5	2	6	3	7	4	8
Condition	Empty	Full	Empty	Full	Empty	Full	Empty	Full
Inner diameter (m)	17.5		28		17.5		28	
Height (m)	45		25		45		25	
Slenderness ratio (H/D)	2.57		0.89		2.57		0.89	
Capacity (kg)	11295780		11272450		11295780		11272450	
Base Type	Fixed		Fixed		Isolated		Isolated	

2.2. Distribution of Masses

Housner [15] studied the dynamic behavior of water tanks, identifying the presence of impulsive mass, which oscillates with the tank, and convective mass, which vibrates independently and collides with the tank walls. The same concept applies to silos, but new equations were required to describe the dynamic response of the stored material, as its behavior differs from that of water. Consequently, the equations proposed by Duan et al. [16] and Lopez and Fernandez-Davila [17] were used to distribute the masses of the defined models, providing the percentage of impulsive mass in the silo, with the remainder being considered convective mass. The required material properties for cement were obtained from the EN 1991-4 code [14] to apply these equations. For slender silos, the results were 65% and 104.68% using the equations of Duan et al. [16] and Lopez and Fernandez-Davila [17], respectively. In the same order, for squat silos, the results were 93.56% and 105.83%. The discrepancies in the percentages of impulsive mass arise because these equations were developed for granular materials, which differ from cement in properties such as particle size, cohesiveness, and particle interactions. Therefore, an impulsive mass percentage of 90% was adopted, based on the average of all results obtained.

2.3. Numerical Model

The stored material and the silo walls were modeled using solid and shell elements, respectively [18]. Figs. 1(a) to 1(c) show Models 7, 8, and the stored material-structure connection details, respectively. Gap elements were employed to simulate the interaction between the stored material and the structure. These are a type of link element that only transmits forces when compressed [19]. Gap elements were used at the connection between the convective mass and the silo walls, as well as at the interface between the convective and impulsive masses, preventing the transmission of

unrealistic tensions to the structure during the oscillation of the convective mass. Only Models 7 and 8 are presented, as these served as the basis for defining the other models by varying the base type and the amount of stored material. Lastly, the 3D elements representing the impulsive mass share common nodes with the shell elements representing the walls, allowing them to vibrate in unison.

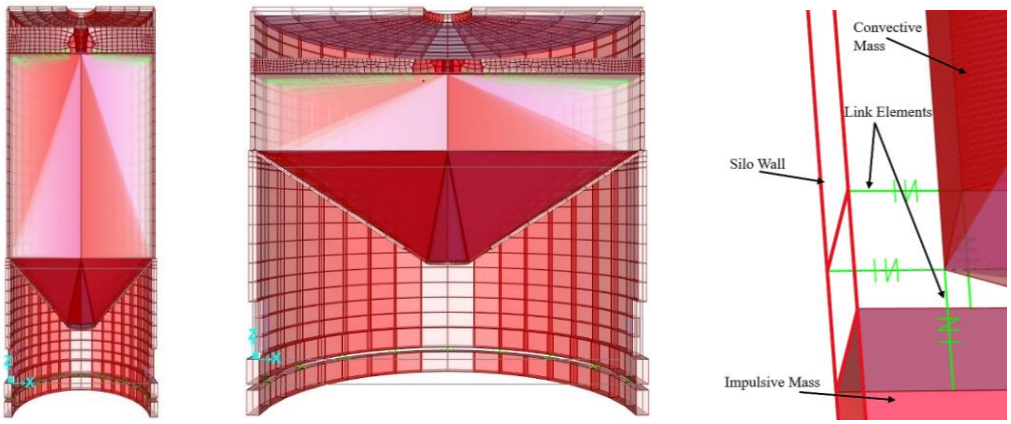

(a) (b) (c)

Fig. 1: Numerical Models 7 (a), 8 (b) and SMSI detail (c)

2.4. Validation

The numerical model validation was carried out by comparing the shear stresses obtained from numerical models 5 and 6, derived from a modal spectral analysis, with the analytical shear stresses obtained from the theory of Silvestri *et al*. [20]. The stress compared from the model corresponded to S22 in Fig. 2(a), as they align in direction with the shear stress of Silvestri et al. [20] when the shell element is oriented vertically. The seismic demand used was based on the Peruvian Code E.030 [21] for a silo located on the coast over rigid soil. The evaluation was conducted at one-meter intervals along the height of the silo body, where the material was stored. The error percentage at a given height was calculated as the average of the errors of the stresses measured every 10° along the perimeter of the silo. The results are presented in Fig. 2(b). At the perimeter level, numerical and analytical stresses tended to decrease as they moved away from orthogonal positions. However, the numerical stresses recovered and increased in value earlier than the analytical stresses. Furthermore, this behavior is consistent along the height, i.e. both types of stress decreased as the evaluation height increased, but the numerical stress decreased to a lesser extent than the analytical stresses. For these reasons, the error percentages tended to increase with height, and acceptable error percentages below 15% were found at the lower levels of both models. The base of the silo body is where the maximum pressures and seismic actions induced by the stored material develop. Therefore, to verify whether the effects of the SMSI are reduced, it was only necessary to evaluate the reduction of seismic actions in the most demanding areas affected by this interaction. Consequently, the error percentages provided by the numerical models were deemed acceptable for this research, which focuses on comparing the reduction of maximum seismic actions that are concentrated in the silo regions with the lowest error percentages. Finally, the increase in error can be attributed to the fact that the formulas of Silvestri et al. [20] were developed considering granular materials with different properties from cement, the absence of convective mass, the use of a 2D analysis in the formulas, and the use of a 3D analysis in the numerical models.

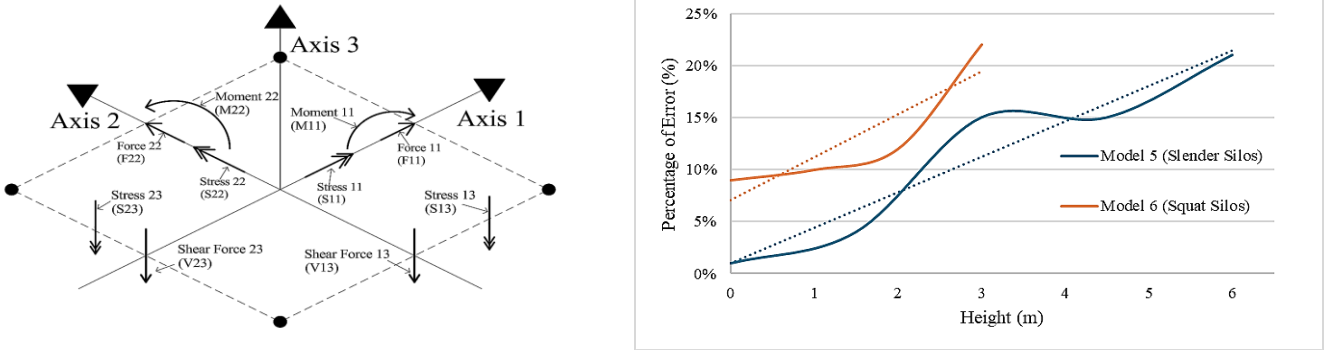

(a) (b)

Fig. 2: Distribution of forces and stresses in a shell element (a) and percentages of error of numerical models (b)

2.5. Performed Analysis and Seismic Loads

A nonlinear dynamic time-history analysis was performed because it accurately captures the seismic response of a structure, making it suitable for evaluating complex structures such as isolated ones. Seven pairs of seismic records were used by the Peruvian Code E.031 [22], with their characteristics presented in Table 2. The models were subjected to the East-West and North-South components simultaneously.

Table 2: Selected acceleration seismic records

ID	Accelerograph Station	Location	Soil Type	Year	Magnitude (Mw)
S1	Parque de la Reserva	Lima-Cercado de Lima	Rigid	1951	6.1
S2	Parque de la Reserva	Lima-Cercado de Lima	Rigid	1966	8.1
S3	Parque de la Reserva	Lima-Cercado de Lima	Rigid	1970	6.9
S4	Parque de la Reserva	Lima-Cercado de Lima	Rigid	1974-January	6.5
S5	Parque de la Reserva	Lima-Cercado de Lima	Rigid	1974-October	8.1
S6	Jorge Alva Hurtado	Lima-Rímac	Rigid	2007	7.9
S7	Ancón	Lima-Ancón	Partially Rigid	2018	5.8

2.6. Target Spectrum and Properties of TFPS

The accelerograms were scaled to the target spectrum defined by the Peruvian Code E.031 [22] for a silo located in Lima on rigid soil using the algorithm by Al Atik and Abrahamson [23]. Fig. 3(a) shows the scaled spectrum, the target spectrum, and the average spectrum of all records. The average spectrum of all records was calculated to demonstrate that the scaling process adequately represents the site conditions defined. Lastly, the time-history record of the East-West component of S4 is shown in Fig. 3(b), as it was selected as a critical case for isolated structures due to presenting the maximum acceleration at the beginning of the record. Additionally, it can be observed that the unscaled record exhibits a similar distribution of accelerations compared to the scaled one, i.e., there was no significant loss of frequencies, and the peaks align with the unscaled record. The North-South component of S4 also exhibited this characteristic. The remaining cases were referred to as non-critical.

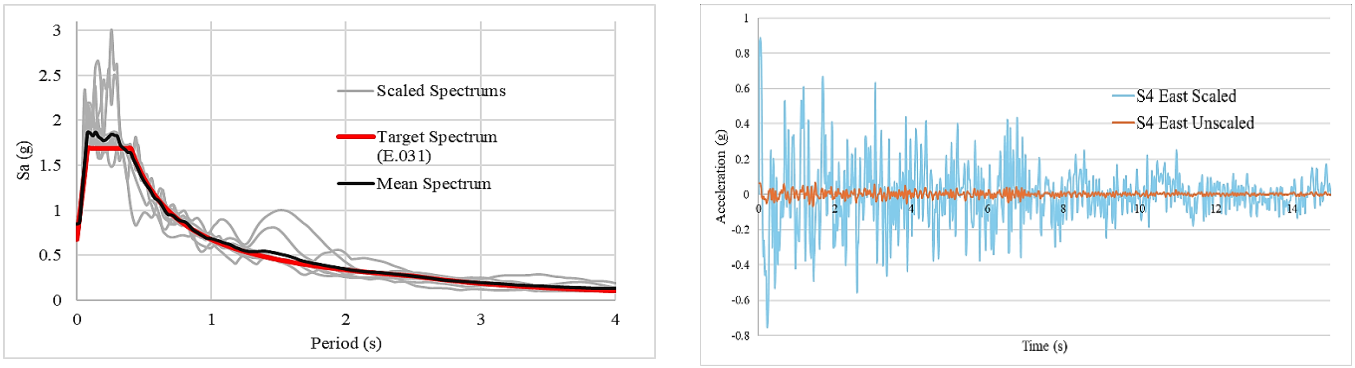

(a) (b)

Fig. 3: Scaled Spectra: (a) Target Spectrum, and Mean Spectrum, and (b) the time-history record of the East-West component of S4.

The characteristics of the TFPS isolators are presented in Table 3. Their geometry and friction coefficients were derived from Sarkisian *et al.* [24] and adjusted using the equations by Fenz and Constantinou [11], ensuring that the lateral displacements induced by seismic actions do not exceed Phase III. This is a common design practice for TFPS isolators, as Phases IV and V are reserved for safety considerations. Lastly, one isolator was defined for slender silos and another for compact isolated silos, as their design weights differed.

Table 3: Characteristics of the TFPS isolators

Property	**Type of Silo**	**External Surfaces**		**Inner Surfaces**	
		Upper Bound	**Lower Bound**	**Upper Bound**	**Lower Bound**
Diameter (m)	Slender	3	3	0.7	0.7
	Squat	2.25	2.25	0.75	0.75
Rigidity (kN/m)	Slender	27647464.7	18809340.7	11330928.1	11330928.1
	Squat	7265350.47	4942820.4	2977602.65	2977602.65
Friction Coefficient – Slow	Slender	0.061	0.042	0.025	0.025
	Squat				
Friction Coefficient – Fast	Slender	0.122	0.083	0.05	0.05
	Squat				
Rate parameter (seg/m)	Slender	110.49	110.49	50	50
	Squat	110.49	110.49	50	50
Sliding Surface Radius (m)	Slender	5	5	0.7	0.7
	Squat	4.65	4.65	0.7	0.7
Stop Distance (m)	Slender	1.13	1.13	0.168	0.168
	Squat	0.74	0.74	0.168	0.168

4. Discussion of the results

The forces and stresses evaluated follow the distribution shown in Fig. 2(a). Figs. 4(a) and 4(b) present the averages of the percentage reductions in the maximum value observed for non-critical cases in a fixed-base model and its equivalent isolated-base model for each type of force and stress, respectively. A negative percentage indicates that there is an increase in seismic action rather than a decrease. Figs. 4(c) and 4(d) are equivalent to Figs. 4(a) and 4(b) but only for the S4 earthquake, as was the critical case analyzed. The percentage ratio between the displacement limit of Phase III in the isolated models and the maximum displacement recorded for each earthquake was calculated, as shown in Fig. 4(e).

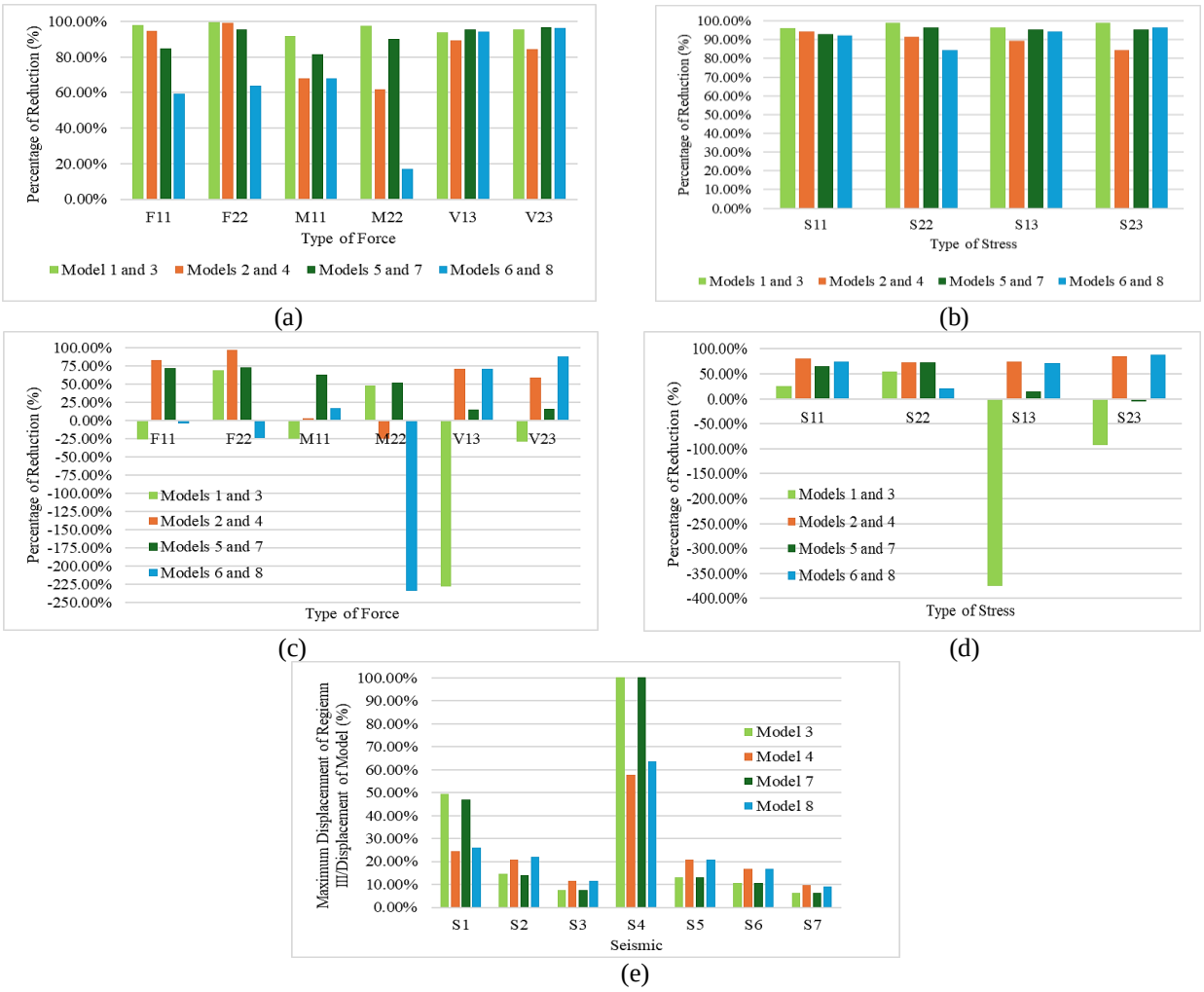

Fig.4: Results: (a, b) Percentage of seismic forces reduction and stress for non-critical cases, (c, d) percentage of reduction of seismic forces and stresses for seismic S4, (e) percentage consumption of the maximum displacement in Phase III of the TFPS relative to the maximum displacement of the model.

The effects of slenderness ratio and SMSI on the addition of unknown dynamic actions were almost completely mitigated for slender silos, both empty (1 and 3) and full (5 and 7), as shown in Figs. 4(a) and 4(b). Seismic actions were reduced by 80% to 99% for non-critical cases, confirming the effectiveness of TFPS isolation systems in such geometries. For squat silos, the reduction in seismic forces and stresses for empty models (2 and 4) ranged from 60% to 98% for non-critical cases, indicating reduced isolation efficiency in this configuration. The reduction was even less efficient for compact full silos (6 and 8), where SMSI was present, achieving only a 20% reduction for the vertical moment M22. This lower efficiency in compact silos aligns with previous observations in other compact storage structures with isolation systems, such as water tanks [25]. The reduced efficiency in mitigating seismic effects in squat silos can be attributed to the uplift of the TFPS isolators. This uplift resulted from instability caused by the lateral displacement of the large silo diameter. The compact models demonstrated periods that fell within the range expected to prevent this behaviour in friction isolators [10]. This instability became critical due to the dynamic pressures generated by the SMSI in full compact silos. This diameter value was necessary to achieve compact geometry for storing twelve thousand tons of material. Furthermore, Fig. 4(e) demonstrates that slender and compact isolated models remained within the TFPS Phase III for non-critical cases, contributing to a reduction in seismic action, as this Phase minimizes the development of large lateral forces. For critical case, compact silos - both empty (2 and 4) and full (6 and 8) - showed increases in M22 and a decrease in seismic action mitigation efficiency. In Fig. 4(e), squat silos did not exceed the TFPS Phase III; however, they exhibited significantly larger displacements compared to non-critical cases, which intensified

the instability effects in these models. Consequently, TFPS isolator uplift increased, leading to higher M22 values and reduced seismic action mitigation efficiency. Additionally, in full compact silos, this seismic response was amplified by dynamic pressures from SMSI, explaining the substantial increase in M22 and other seismic actions, such as F11 and F22. It should be noted the effects observed in squat silos may be attributed to simplifications in the numerical model, which was calibrated only to match overall seismic actions and not the secondary effects induced by SMSI. In slender empty silos (1 and 3), the shear force V13 doubled, while other seismic forces, such as F11, experienced a smaller increase. As shown in Fig. 4(e), models 1 and 3 exceeded TFPS lateral displacement Phase III, briefly transitioning into Phase V. Large displacements are expected in isolated structures subjected to pulses, such as near-fault earthquakes [26], or, in this case, an earthquake with peak acceleration occurring near 0 seconds. In this Phase, minor increases in lateral displacement can lead to substantial increases in the lateral force generated by TFPS isolators, as described by the equations of Fenz and Constantinou [11]. The transfer of lateral forces from the isolation interface to the superstructure increased seismic actions for slender empty silos. However, for slender full silos (5 and 7), despite TFPS isolators also transitioning from Phase III to V under earthquake S4 (Fig. 4(e)), no significant increases in seismic forces (Fig. 4(c)) or stresses (Fig. 4(d)) were observed. The only difference was the presence of stored material, suggesting that the improved seismic action reduction in slender full silos under extreme conditions was due to the added stiffness provided by the stored material, like that observed by Lopez and Fernandez-Davila [17].

5. Conclusions

This article examined the impact of the Slenderness Ratio and SMSI on isolated silos using TFPS. The study employed eight parametric models and analysed seven seismic records using nonlinear time-history analyses. The findings revealed that TFPS significantly reduced seismic forces and stresses in slender silos. Therefore, the effects of Slenderness Ratio and SMSI are generally negligible for slender silos with TFPS in non-critical scenarios. In contrast, TFPS effectiveness was less pronounced in squat silos, where secondary effects of SMSI developed; however, it is essential to assess the evaluated parameters as the numerical models were not calibrated with sufficient accuracy to simulate those effects. In a critical situation, both empty and full slender silos exhibited significant lateral displacements, which led to excessive seismic actions. Nevertheless, the additional stiffness provided by the stored material in full slender silos mitigated these actions, ensuring that reduction levels remained within acceptable limits. The squat silos exhibited the same seismic response for non-critical cases, but large lateral displacements intensified it. Thus, full slender silos have shown the best seismic response with TFPS under any seismic event. These findings provide a robust framework for optimizing the design of base-isolated reinforced concrete silos.

Acknowledgments

We thank the Peruvian University of Applied Sciences for supporting and funding this research through the UPC-EXPOST-2025-1 incentive.

References

[1] H. Jing, H. Chen, J. Yang, and P. Li, “Shaking table tests on a small-scale steel cylindrical silo model in different filling conditions,” *Structures*, vol. 37, pp. 698-708, 2022.

[2] J. Yang, G. Feng, H. Jing, and F. Zhang, “Seismic response and theoretical analysis of grain bulk material-steel silo structure under earthquake action,” *Journal of Constructional Steel Research*, vol. 211, 2023.

[3] A. Durmus and R. Livaoğlu, “The role of slenderness on the seismic behavior of ground-supported cylindrical silos,” *Advances in Concrete Construction*, vol. 7, no. 2, pp. 65-74, 2019.

[4] A. Durmus and R. Livaoğlu, “Simplified seismic response model for a bulk solid-silo-embedded foundation/soil system,” *Soil Dynamics and Earthquake Engineering*, vol. 165, 2022.

[5] A. Durmus and R. Livaoğlu, “SSI effects on seismic response of RC flat-bottom circular silos,” *Structures*, vol. 57, 2023.

[6] M. Furinghetti, S. Mansour, M. Marra, S. Silvestri, I. Lanese, F. Weber and A. Pavese, “Shaking table tests of a full-scale base-isolated flat-bottom steel silo equipped with curved surface slider bearings,” *Soil Dynamics and Earthquake Engineering*, vol. 176, 2024.

[7] D. Bîtcă, E. Ursu and P. Ioan, “Seismic Base Isolators for a Silo Supporting Structure,” *Mathematical Modelling in Civil Engineering*, vol. 11, no.2, 2015.

[8] Y. Xu, T. Becker, and T. Guo, "Design optimization of triple friction pendulums for high-rise buildings considering both seismic and wind loads," *Soil Dynamics and Earthquake Engineering*, vol. 142, 2021.
[9] Y. Xu, T. Guo, J. Xiong, B. Chen, Q. Zhi and J. Yang, "Optimization design of triple friction pendulums for Base-isolated High-rise buildings based on bearing displacement and collapse fragility," *Structures*, vol. 43, pp. 1091-1099, 2022.
[10] G. Auad, J. Almazán, and F. Vilca, "Comparative analysis of the dynamic of structures equipped with cylindrical and spherical frictional bearings subjected to near-fault earthquakes," *Structures*, vol. 60, pp. 1293-1310, 2024
[11] D. Fenz and C. Constantinou, "Spherical sliding isolation bearings with adaptive behavior: Theory," *Earthquake Engineering and Structural Dynamics*, vol. 37, pp. 163-183, 2008.
[12] A. Vibhute, S. Bharti, M. Shrimali and T. Datta, "Performance evaluation of FPS and LRB isolated frames under main and aftershocks of an earthquake," *Structures*, vol. 44, pp. 1532-1545, 2022.
[13] P. Conde, O. Gauron, A. Saidou, A. Busson and P. Paultre, "Probabilistic lateral stability and shear failure limit states of bridge natural rubber bearings," *Engineering Structures*, vol. 289, 2023.
[14] EN 1991-4, "Eurocode 1: Actions on Structures – Part 4: Silos and Tanks," *European Committee for Standardization*, Brussels, Belgium, 2006.
[15] G. Housner, "Dynamic Pressures on Accelerated Fluid Containers," *Bulletin of the Seismological Society of America*, vol. 47, no.1, pp. 15-35, 1957.
[16] J. Duan, Y. Han, and D. Li, "The Dynamic Behavior of Silos with Grain-like Material during Earthquakes," *Sustainability*, vol. 15, 2023.
[17] A. Lopez and V. Fernandez-Davila, "Simplified Method for Evaluating Seismic Response of Circular Reinforced Concrete Silos," in *16th World Conference on Earthquake Engineering*, Santiago, Chile, 2017.
[18] CSI, "SAP2000: Integrated Software for Structural Analysis and Design," Berkeley, CA, USA: Computers and Structures, Inc., 2023
[19] Computers and Structures, Inc., "CSi Analysis Reference Manual," Berkeley, CA, USA, 2017.
[20] S. Silvestri, G. Gasparini, T. Trombetti and D. Foti, "On the evaluation of the horizontal forces produced by grain-like material inside silos during earthquakes," *Bulletin of Earthquake Engineering*, vol. 10, no. 5, 2012.
[21] Ministerio de Vivienda, Construcción y Saneamiento, "Norma E.030 Diseño Sismorresistente," *Reglamento Nacional de Edificaciones*, Lima, Perú, 2018.
[22] Ministerio de Vivienda, Construcción y Saneamiento, "Norma E.031 Aislamiento Sísmico," *Reglamento Nacional de Edificaciones*, Lima, Perú, 2019.
[23] L. Al Atik and N. Abrahamson, "An Improved Method for Nonstationary Spectral Matching," *Earthquake Spectra*, vol. 26, no. 3, pp. 601-617, 2010.
[24] M. Sarkisian, P. Lee, L. Hu, C. Doo, V. Zayas, M. Constantinou, and R. Bachman, "Property Verification of Triple Pendulum Seismic Isolation Bearings," in *20th Analysis & Computation Specialty Conference*, Illinois, USA, 2012.
[25] A. Saria, M. Djermane, and N. Hadj-Djelloul, "Three-Dimensional Nonlinear Dynamic Analysis of Base Isolated Cylindrical Steel Tank," *Civil Engineering Journal*, vol.8, no. 6, 2022.
[26] N. Günes, "Effects of near-fault pulse-like ground motions on seismically isolated buildings," *Journal of Building Engineering*, vol. 52, 2022